frontiers | Frontiers in Chemistry

ORIGINAL RESEARCH
published: 29 April 2022
doi: 10.3389/fchem.2022.904241

Bimetallic Cobalt–Copper Nanoparticle-Decorated Hollow Carbon Nanofibers for Efficient CO_2 Electroreduction

Congyi He, Siyu Wang, Xingxing Jiang, Qi Hu, Hengpan Yang and Chuanxin He**

College of Chemistry and Environmental Engineering, Shenzhen University, Shenzhen, China

Bimetallic materials are one of the most promising catalysts for the electrochemical reduction of CO_2, but there are still many challenges to be overcome on the route to industrialization. Herein, a series of carbon nanofiber-supported bimetallic cobalt–copper catalysts (Co_xCu_y/CFs) are designed and constructed through the electrospinning technique and a subsequent pyrolysis procedure. Small-sized Co–Cu nanoparticles are homogenously distributed on the porous carbon nanofibers, which can significantly improve the utilization rate of metal sites and greatly reduce the loading amount of metals. Moreover, different product distributions and catalytic performance can be obtained in CO_2 reduction *via* adjusting the metal proportion of Co_xCu_y/CFs. Especially, Co_3Cu/CFs can bring forth a 97% total faradaic efficiency (FE) of CO (68%) and HCOOH (29%) at −0.8 V_{RHE} cathode potential in 0.5 M $KHCO_3$ electrolyte. Furthermore, the hierarchical pores can firmly confine the small Co–Cu nanoparticles and keep them from easy agglomeration during electrolysis, eventually leading to 60 h of stability for Co_3Cu/CFs in CO_2 electroreduction. This study might provide a facile and economic method to fabricate efficient bimetallic catalysts for CO_2 electroreduction and other electrocatalysis applications.

Keywords: bimetallic catalysts, copper–cobalt bimetal, carbon nanofibers, CO_2 reduction, Electrocatalysis

OPEN ACCESS

Edited by:
Jie Zeng,
University of Science and Technology of China, China

Reviewed by:
Zhigang Geng,
University of Science and Technology of China, China
Hongwen Huang,
Hunan University, China

****Correspondence:***
Hengpan Yang
hpyang@szu.edu.cn
Chuanxin He
hecx@szu.edu.cn

Specialty section:
This article was submitted to Electrochemistry, a section of the journal Frontiers in Chemistry

Received: *25 March 2022*
Accepted: *04 April 2022*
Published: *29 April 2022*

Citation:
He C, Wang S, Jiang X, Hu Q, Yang H and He C (2022) Bimetallic Cobalt–Copper Nanoparticle-Decorated Hollow Carbon Nanofibers for Efficient CO_2 Electroreduction. Front. Chem. 10:904241. doi: 10.3389/fchem.2022.904241

INTRODUCTION

CO_2 electroreduction can convert greenhouse gas CO_2 into renewable fuels and industrial building-block chemicals, which has been advocated as a promising candidate for the artificial carbon cycle (Qiao et al., 2014; Sharifian et al., 2021; Zhang et al., 2021). Electrochemical reduction of CO_2 can be motivated by vast amounts of excess electricity from renewable energy resources, for example, wind, tide, and solar power plants (Benson et al., 2009; Fu et al., 2019). However, the CO_2 molecule has a very high chemical stability; hence, appropriate catalysts are needed to activate them (Hori et al., 2008; Appel et al., 2013).

Therefore, a series of catalysts have been constructed to enhance the efficiency of CO_2 electroreduction, including molecular catalysts (Appel and Helm, 2014; Nichols and Machan, 2019; and Bonin et al., 2017), heterodoped carbon catalysts (Sun, 2021; Kumar et al., 2013), oxide-derived catalysts (Duan et al., 2021; Duan et al., 2018), single-atom catalysts (Yang et al., 2019; Chen Jia et al., 2021; Wei et al., 2022; and Zhang et al., 2022), and multimetallic catalysts (Lin Jia et al., 2021; Vasileff et al., 2018; and Jia et al., 2022). Among these available catalysts, bimetallic catalysts

have exhibited remarkable performance in CO_2 reduction. Bimetallic materials not only change the electronic structures of the single component (Yang et al., 2021) but also create new active sites to regulate the binding energy of key intermediates during CO_2 reduction (Jeoung and Dobbek, 2007; Yu et al., 2021; Cheng et al., 2021). Meanwhile, carbon materials (e.g., carbon black, graphite powder, and carbon nanotubes) are utilized as supports or carriers for bimetallic catalysts in actual electrolysis, which can improve the dispersion and conductivity (Jia et al., 2022). However, these carbon materials need pretreatment, including purification or surface functionalization, which might damage the porous structure and electrical conductivity (Liu et al., 2014). Therefore, it is still urgent to design a simple and effective approach to carbon supported with excellent activity in CO_2 electroreduction.

In this study, we report the facile synthesis of several Co–Cu bimetallic catalysts, that is, Co–Cu bimetallic nanoparticles/porous carbon nanofiber (Co_xCu_y/CF) composites using the electrospinning technique and thermal treatment. In the composites, Co_xCu_y nanoparticles are uniformly and stably dispersed on the abundant poles of carbon nanofibers, rather than simply being absorbed or drop-coated on the surface. This structure can largely expose the Co_xCu_y nanoparticles onto the reaction interface of CO_2 electroreduction and greatly improve the efficiency of electronic transmission. Furthermore, we also systematically investigated the effect of the mole ratio of Co and Cu components on the product distribution and faradaic efficiency. The results indicated that the Co_3Cu/CF catalyst with a mole ratio of 3:1 displayed an outstanding catalytic activity and long-term stability in CO_2 electroreduction.

MATERIALS AND METHODS

Chemicals and Characterizations

All reagents were used as received without further purification.

Electrochemical tests were performed with a CHI 760e electrochemical Station (Shanghai Chenhua Instruments Company). Gaseous products were detected by gas chromatography (Shimadzu, GC-2014c) with a flame ionization detector (FID) and a thermal conductivity detector (TCD). Liquid products were detected using a nuclear magnetic resonance spectrometer (NMR, Ascend 400, Bruker, Germany). The micromorphology, crystalline structure, and element mapping were obtained by a field emission scanning electron microscope (FE-SEM, FEI JEOL-7800F) and a high-resolution transmission electron microscope (HR-TEM, JEM-2100F). The metal amount in the as-synthesized catalyst was detected using inductively coupled plasma-optical emission spectrometry (ICP-OES, OPTIMA2100DV). N_2 adsorption/desorption curves were achieved by a specific surface and porosity analyzer (Micromeritics ASAP 2460) and calculated using the Brunauer–Emmett–Teller (BET) equation. X-ray diffraction (XRD) patterns were recorded with an X-ray powder diffractometer (Rigaku MiniFlex 600) with Cu Kα radiation (k = 1.5406 Å). Raman spectra were acquired with a laser Raman spectrometer (LabRAM HR Evolution, HORBIA FRANCE SAS) with a 633-nm laser excitation. X-ray photoelectron spectra (XPS) were recorded on an X-ray photoelectron spectrometer (ThermoVG Scientific ESCALAB 250) with Al Kα X-ray as the source.

Synthesis of Catalysts

All the five samples in this study were prepared by electrospinning technology. The preparation steps are as follows: 7 ml of N, N-dimethylformamide, 0.5 g polyacrylonitrile (PAN), and 0.75 g ZIF-8 nanoparticles were put into a beaker and stirred until they were evenly mixed into a white viscous solution. Then, 0.2183 g of $Co(NO_3)_2{\cdot}6H_2O$ (0.00075 mol) and 0.061 g of $Cu(NO_3)_2{\cdot}3H_2O$ (0.00025 mol) were added, and stirring was continued for at least 20 h or until the mixture was fully mixed to obtain a purple viscous spinning precursor solution. This precursor solution was injected into the syringe and electrospun to polymer fibers. After spinning, the polymer fibers were put into vacuum drying oven at 60°C for at least 12 h, and the dried polymer fiber was pre-oxidized in a muffle furnace. Then those pre-oxidized fibers were carbonized in nitrogen atmosphere. The initial temperature was set at 25°C, raised to 900°C at the rate of 5°C/min, and maintained for another 2 h. The as-synthesized catalyst was named as Co_3Cu/CFs.

Another four catalysts with different metal ratios can be obtained by changing the molar ratio of metal precursors Co $(NO_3)_2{\cdot}6H_2O$ and Cu $(NO_3)_2{\cdot}3H_2O$, including 1/0, 1/1, 1/3, and 0/1. The as-prepared samples were named as Co/CFs, CoCu/CFs, $CoCu_3$/CFs, and Cu/CFs.

Electrochemical Measurements

All the five catalysts were powdered and drop-coated onto a carbon paper (SGL Carbon Corporate) to get a useful working electrode. CO_2 reduction activity was tested in a typical H-type electrochemical cell separated by an anion exchange membrane between anodic and cathodic chambers, with a Pt foil as the counter electrode and an Ag/AgCl as the reference electrode; 0.5 M $KHCO_3$ solution was employed as the electrolyte and bubbled with high purity CO_2 or N_2 (99.995%). The original potentials measured in this manuscript were converted to the reversible hydrogen electrode (RHE) *via* the Nernst equation:

$$E(RHE) = E(Ag/AgCl) + 0.199 + 0.059 \times pH. \quad (1)$$

Products from CO_2 reduction were analyzed at various cathodic potentials with a fixed time of 15 min, and the gaseous components were directly injected into gas chromatography. The liquid-phase products were detected *via* ^{1}H NMR spectra. The Faraday efficiencies of the products were calculated *via* the following equations. Q is the total charge transferred through the working electrode at different potentials; m is the number of electrons transferred, which is 2 for HCOOH, CO, and H_2, and 8 for CH_4; n is the mole numbers of products; and F is the Faradaic constant (96,485 C mol^{-1}).

$$FE = \frac{Q_{product}}{Q_{total}} = \frac{m \times n \times F}{Q_{total}} \quad (2)$$

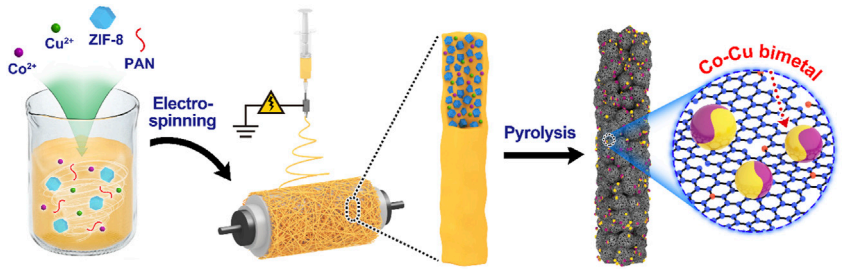

FIGURE 1 | Synthesis strategy of Co–Cu bimetallic nanoparticle-decorated carbon nanofibers.

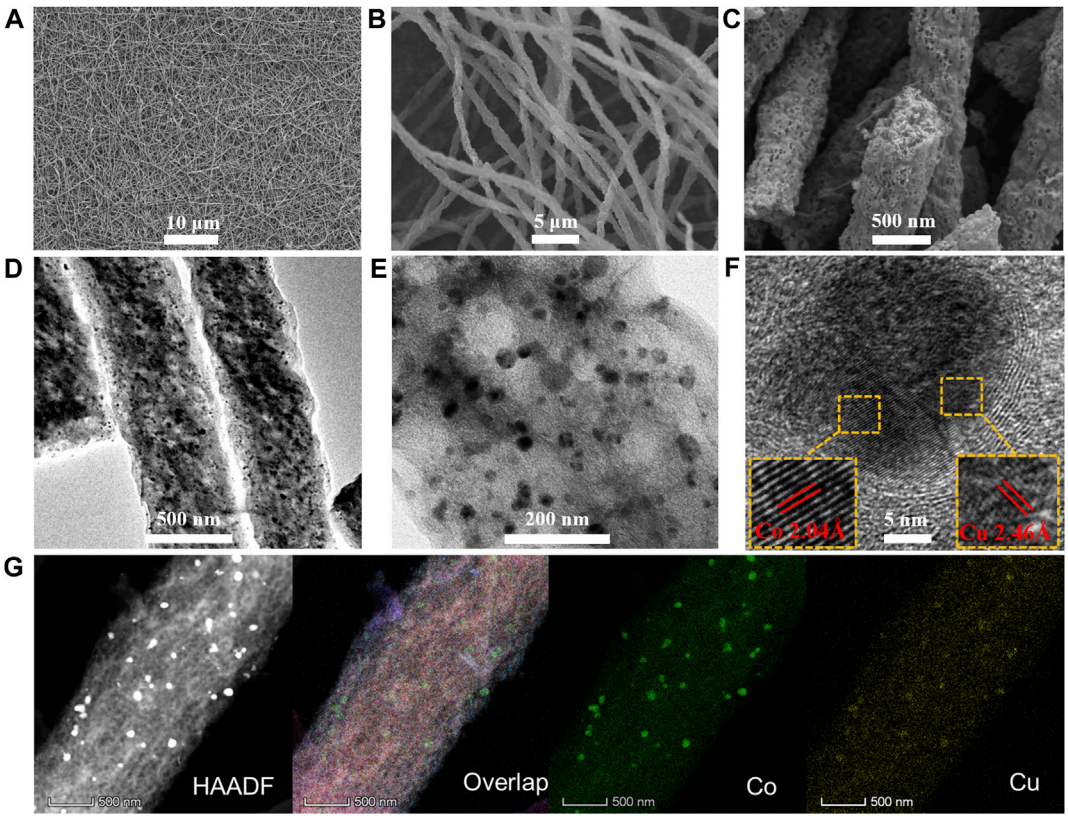

FIGURE 2 | (A–C) SEM and **(D–E)** TEM images with different resolutions of Co_3Cu/CFs, respectively; **(F)** HR-TEM images of Co_3Cu/CFs: inset shows the lattice fringes of Co and Cu; **(G)** HAADF-STEM and elemental mapping images of Co_3Cu/CFs.

RESULTS AND DISCUSSIONS

Characterizations of Catalysts

The specific preparation process of the material is described in **Figure 1**. First, $Co(NO_3)_2{\cdot}6H_2O$, $Cu(NO_3)_2{\cdot}3H_2O$, ZIF-8 nanoparticles as well as PAN were dissolved in DMF to prepare a precursor solution, and then an electrospinning technology was used under constant conditions to get PAN nanofibers with different Co/Cu mole ratios. Then, the Co–Cu/PAN nanofibers were heated to 900°C under a N_2 atmosphere for carbonization. Notably, there are no extra surfactants or reductants involved in the whole procedure. The polymer linkers were pyrolyzed and carbonized to generate the main body of carbon nanofibers, and ZIF-8 nanoparticles collapsed to form the abundant mesopores and macropores through these nanofibers (Yang et al., 2020a). Co^{2+} and Cu^{2+} ions were reduced by organic linkers, and the bimetallic nanoparticles were engendered with a smaller particle size due to the confinement of the polymer and ZIF-8 nanoparticles. The compositions of these bimetallic nanoparticles were tuned by the feeding ratio of $Co(NO_3)_2{\cdot}6H_2O$ and $Cu(NO_3)_2{\cdot}3H_2O$ precursors, eventually generating Co_3Cu/CFs, Co/CFs, CoCu/CFs, $CoCu_3$/CFs, and Cu/CFs.

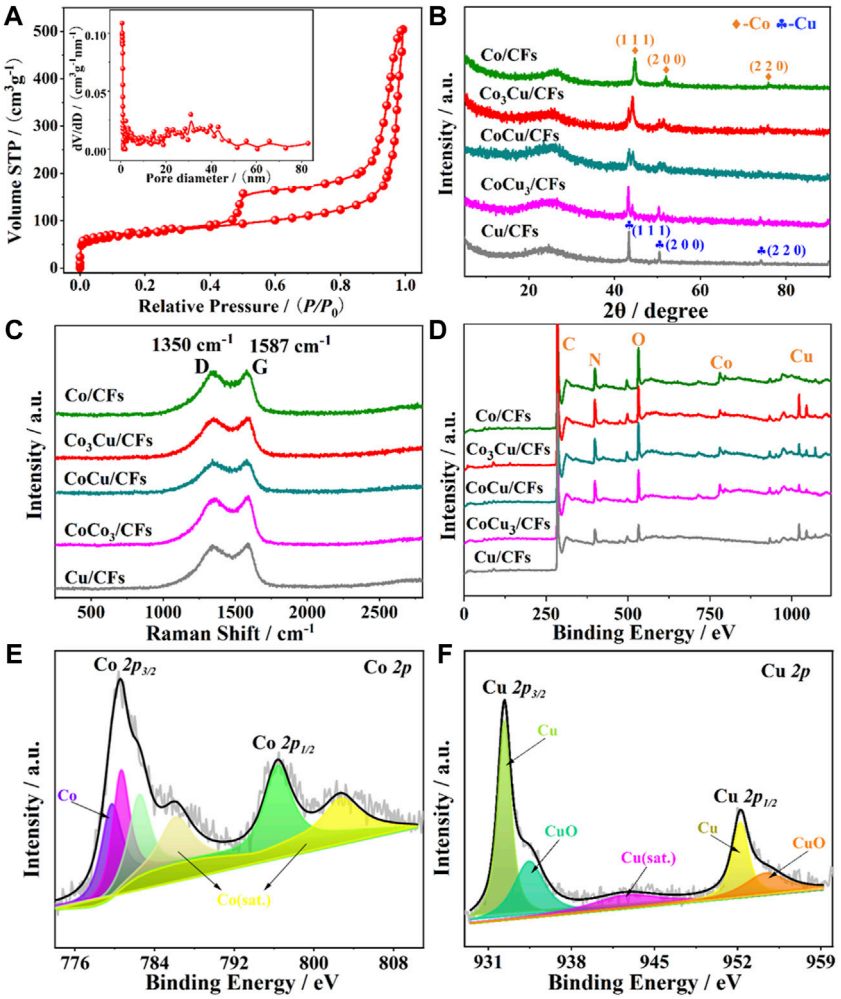

FIGURE 3 | (A) N_2 sorption isotherms of Co_3Cu/CFs: inset displays the pore size distribution; **(B)** XRD patterns, **(C)** Raman spectra, and **(D)** XPS survey spectra of the five catalysts; **(E)** Co *2p* and **(F)** Cu *2p* fine XPS spectra of Co_3Cu/CFs.

As shown in **Figure 2**, the surface morphology and nanostructure of the as-synthesized Co_3Cu/CF catalyst were recorded by FE-SEM and HR-TEM, respectively. The diameter of the carbon nanofibers in Co_3Cu/CFs ranges from 500 to 600 nm. The length is in the scale of hundreds of micrometers, and the interlaced nanofibers furtherly form a network structure (**Figures 2A,B**). Moreover, abundant hollow pores, in the size range of dozens of nanometers, could be easily seen throughout Co_3Cu/CFs (**Figures 2C,D**). N_2 sorption isotherms (**Figure 3A**) further demonstrate that Co_3Cu/CFs have type Ⅳ sorption isotherm, belonging to the mesoporous structure. Co–Cu nanoparticles, in an ~20 nm diameter range, are evenly immobilized within the hollow pores of carbon nanofibers (**Figures 2D,E**).

In addition, **Figure 2F** shows the clear HR-TEM image of an independent Co–Cu bimetallic nanoparticle, and the interplanar spacing of crystalline lattices marked with red lines is measured as 2.04 Å and 2.46 Å, corresponding to the Co (111) and Cu (111) planes (Liu et al., 2014; Kim et al., 2017), respectively. Furthermore, the high-angle annular dark field STEM (HAADF-STEM) and elemental mapping images indicate that Co_3Cu/CFs contain Co and Cu elements. The good match between the emerging positions of Co and Cu elements directly proves the formation of Co–Cu bimetallic nanoparticles. According to the SEM, HR-TEM (**Supplementary Figure S1,S2**), and N_2 sorption isotherms (**Supplementary Figure S3**, **Supplementary Table S1**), Co/CFs, CoCu/CFs, $CoCu_3$/CFs, and Cu/CFs display similar interlaced nanofibers, abundant hollow pores, and uniform nanoparticles. Hence, the regulation of metal ratio would not significantly change the surface morphology and nanostructure. The actual Co/Cu ratios in the as-synthesized catalyst were detected by ICP-OES. CoCu/CFs, Co_3Cu/CFs, and $CoCu_3$/CFs own Co/Cu ratios of 1/0.95, 3/0.96, and 0.98/3, respectively, which are close to the original ratios in precursor solutions.

As shown in the XRD patterns (**Figure 3B**), the sharp diffraction peaks at 44.9°, 52.5°, and 76.2° can be seen in Co/CF samples, which are attributed to the Co (111), (200), and (220)

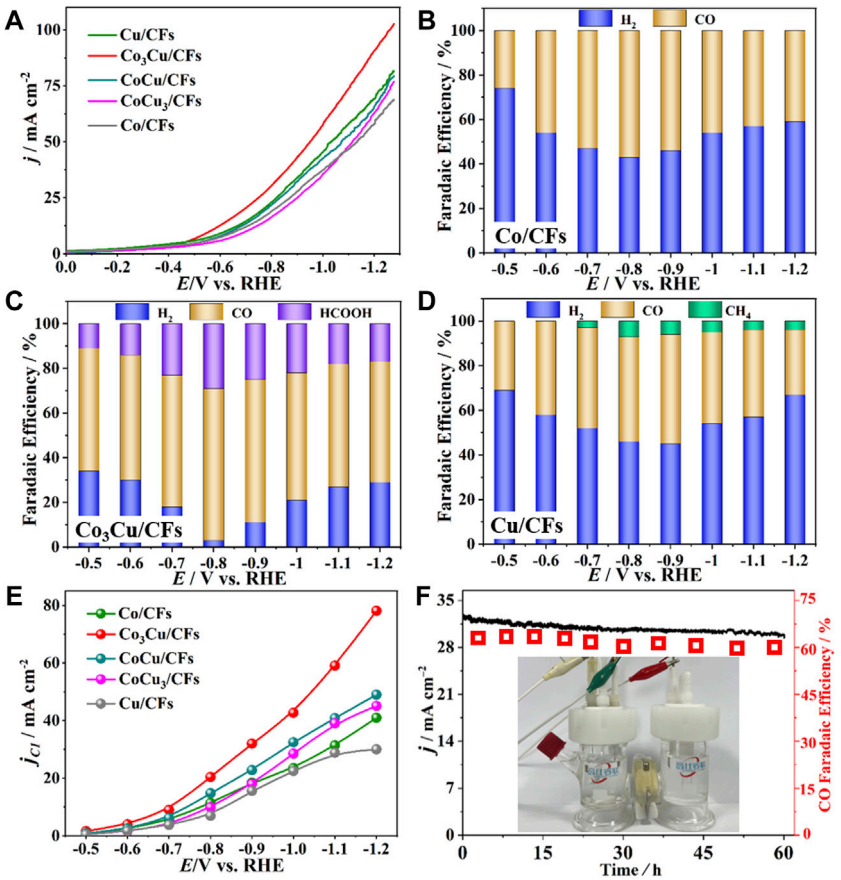

FIGURE 4 | (A) LSV curves of the five samples recorded in a CO_2-saturated 0.5 M $KHCO_3$ electrolyte; Faradaic efficiencies of **(B)** Co/CFs, **(C)** Co_3Cu/CFs, and **(D)** Cu/CFs in a 0.5 M $KHCO_3$ electrolyte; **(E)** C1 product partial current densities of the five samples; **(F)** long-term tests of Co_3Cu/CFs at −0.8 V_{RHE} in a 0.5 M $KHCO_3$ electrolyte.

planes (JCPDS 89-7093), respectively. Those peaks at 43.3°, 50.5°, and 74.2° of the Cu/CF samples are in accordance with the Cu (111), (200), and (220) planes (JCPDS 89-7093), respectively. The XRD patterns of Co_3Cu/CFs, CoCu/CFs, and $CoCu_3$/CFs possess both Co and Cu diffraction peaks, further verifying the formation of Co–Cu bimetallic nanoparticles. The Raman spectra (**Figure 3C**) of the five samples contain characteristic peaks around 1,350 cm^{-1} and 1,578 cm^{-1}, related to the d band of defective carbon and the G band of graphite carbon (Kumar et al., 2013), respectively. Co_3Cu/CFs have the largest intensity ratio of D and G bands (I_D/I_G, 1.01), indicating more defects and more potential active sites. The survey XPS spectra of Co_3Cu/CFs (**Figure 3D**, **Supplementary Figure S4**) confirm the presence of Co, Cu, C, N, and O elements. The high-resolution Co *2p* XPS spectrum of Co_3Cu/CFs (**Figure 3E**) exhibits four peaks, including Co $2p_{3/2}$ (780.3 eV), Co $2p_{1/2}$ (795.6 eV), and two Co satellite peaks. Two strong peaks in the Cu *2p* XPS spectrum (**Figure 2F**) that appear at 932.3 and 952.0 eV can be indexed to Cu $2p_{3/2}$ and Cu $2p_{1/2}$, respectively. Notably, oxide peaks can be detected in Co and Cu *2p* XPS spectra of Co_3Cu/CFs because of the easy oxidation of metallic Co and Cu nanoparticles (Xie et al., 2021; Kim et al., 2017). Similar C, N, Co, or Cu species could also be observed in the XPS spectra of another four samples (**Supplementary Figure S5–S8**).

CO_2 Electroreduction Tests

The CO_2 electroreduction performances of Co–Cu bimetallic catalysts were investigated and compared with the performance of pure Co or Cu catalysts in a typical H-type electrochemical cell. All the catalysts were pre-activated using cyclic voltammetry until stable profiles were obtained. **Figure 4A** and **Supplementary Figure S9** present the linear sweep voltammetry (LSV) curves of five samples in N_2-saturated or CO_2-saturated 0.5 M $KHCO_3$. The cathodic current densities of all five catalysts were measured to be approximately doubled in CO_2 than those in the N_2-saturated electrolyte, indicating the potential catalytic activity in CO_2 reduction (Zhang et al., 2014). In addition, LSV tests also prove that Co_3Cu/CFs show the highest current density among the five catalysts (**Figure 4A**).

In order to further evaluate the catalytic activities and quantify the product distribution from CO_2 electroreduction, potential dependent CO_2 electrolysis using five catalysts was conducted in a 0.5 M $KHCO_3$ electrolyte from −0.5 V_{RHE} to −1.2 V_{RHE} applied cathode potential. Gas products were directly injected into gas

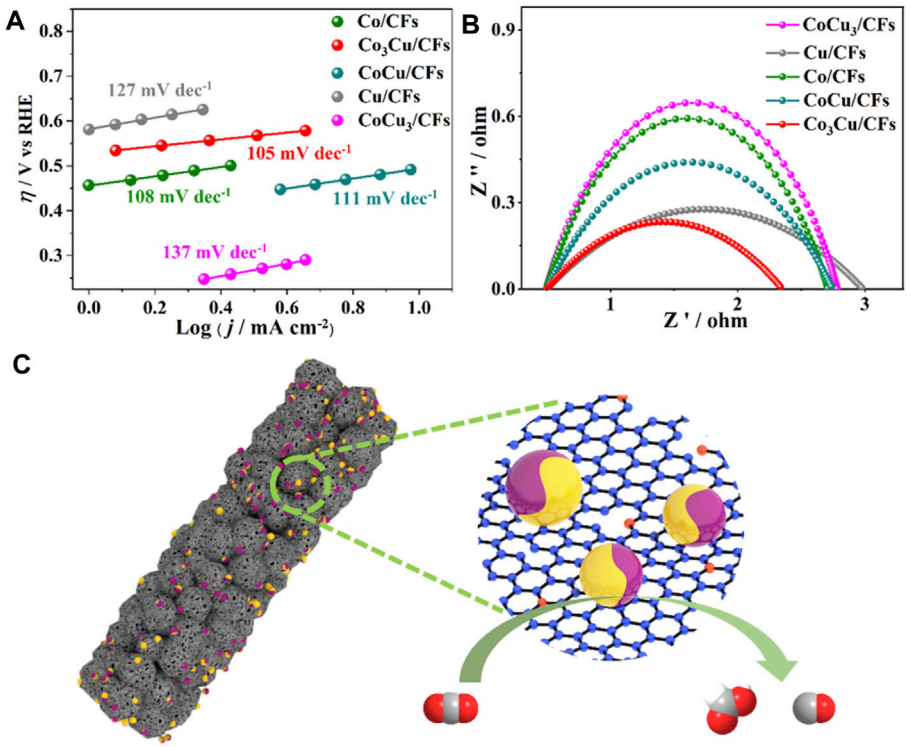

FIGURE 5 | (A) Tafel plots of five samples during the CO_2 electroreduction process; **(B)** EIS Nyquist spectra of the five samples; **(C)** catalytic mechanism of Co_3Cu/CFs for the reduction of CO_2 to CO and HCOOH.

chromatography for on-line analysis, and liquid products in the catholyte were detected using ^1H NMR after each electrolysis. The product distribution and faradaic efficiencies (FEs) are summarized in **Figure 4** and **Supplementary Figure S10**. For comparison of the electrocatalytic activities, Co/CFs and Cu/CFs with pure Co and Cu nanoparticles were also synthesized and assessed in CO_2 electrolysis. As shown in **Figure 4B**, Co/CFs generated CO as the only product from the CO_2 reduction and H_2 from the hydrogen evolution reaction (HER), with a 57% maximum FE for CO at −0.8 V_{RHE} applied potential. As for Cu/CFs (**Figure 4D**), it produced H_2, CO, and CH_4 during electrolysis, with a 49% maximum FE for CO at −0.9 V_{RHE}. CH_4 is one of the urgent products with the transfer of eight electrons (Sharifian et al., 2021); however, highest FEs of CH_4 only reach 7% at −0.8 V_{RHE}. Both Co/CFs and Cu/CFs show certain activities in CO_2 electroreduction, but neither of them could effectively suppress the HER process, and the FEs of H_2 range from 43 to 74%. As displayed in **Figure 4C** and Supplementary Figure S10, doping Co with Cu causes a significant increment in CO_2 catalysis. Compared to Co/CFs and Cu/CFs, the CO_2 reduction procedure on Co_3Cu/CFs, CoCu/CFs, and $CoCu_3$/CFs became much more dominant than the HER procedure. In particular, the maximum FE for C1 production (HCOOH and CO) increases to 97% at −0.8 V_{RHE} using the Co_3Cu/CFs catalyst, and the HER is totally suppressed to only a 3% FE of H_2. CoCu/CFs and $CoCu_3$/CFs have a similar tendency of FEs for CO_2 electrolysis as that of Co_3Cu/CFs, but they acquire lower total FEs of CO and HCOOH throughout the applied potential.

Chronoamperometry (CA) was used to evaluate the total current density during CO_2 electrolysis, and five samples achieved very close total current densities from −0.5 V_{RHE} to −1.2 V_{RHE} (**Supplementary Figure S11**). In addition, the partial current densities (j_{C1}) for C1 products (CO, HCOOH, and CH_4) were normalized by the total current densities and FEs at each cathode potential. Co_3Cu/CFs brought forth a significantly higher partial current density than Co/CFs, Cu/CFs, CoCu/CFs, and $CoCu_3$/CFs within the potential range, and got a maximum j_{C1} of 78.1 mA cm^{-2} at −1.2 V_{RHE} (**Figure 4E**). Therefore, Co_3Cu/CFs possess remarkable catalytic activity in CO_2 reduction, and they can also successfully suppress the HER procedure at relatively high cathode potentials. Moreover, it is extremely important to estimate the long-term durability of bimetallic catalysts because increasing the applied potentials and heavy current densities might seriously impact the structural stability (Vasileff et al., 2018; Jia et al., 2022). Long-term tests of potentiostatic CO_2 electrolysis were conducted using Co_3Cu/CFs catalysts at −0.8 V_{RHE} cathode potential where the best FEs of C1 products were obtained. The gaseous products were detected on-line every 6 h, and the corresponding CO FEs and current densities *versus* time are plotted in **Figure 4F**. Both CO FEs and partial current densities of the Co_3Cu/CF catalyst exhibited only small declines during the 60 h electrolysis, retaining approximately 90% of the original values and manifesting

excellent stability in CO_2 electroreduction. Co_3Cu/CFs were characterized after a long-term electrolysis by TEM (**Supplementary Figure S12**), and the small Co_3Cu/CFs did not agglomerate together. As described previously (**Figures 2D,E**), the Co–Cu bimetallic nanoparticles are uniformly dispersed and firmly confined within the hierarchical pores of carbon nanofibers, and separated from easy agglomeration during electrolysis.

The aforementioned experimental results demonstrate the outstanding activities of Co_3Cu/CFs in CO_2 reduction. The mechanism of the high performance was first investigated using Tafel slopes within sufficiently low overpotential ranges. As presented in **Figure 5A**, 105 mV dec^{-1} Tafel value is observed on Co_3Cu/CFs, confirming the first electron transfer from CO_2 to $CO_2^{\bullet-}$ as the rate determining step (Chen Jia et al., 2021). Compared to those of Co/CFs (108 mV dec^{-1}), Cu/CFs (127 mV dec^{-1}), CoCu/CFs (111 mV dec^{-1}), and $CoCu_3$/CFs (137 mV dec^{-1}), the lower Tafel value of Co_3Cu/CFs indicates faster reaction kinetics in CO_2 reduction. As mentioned previously, four electron product CH_4 was only obtained with the Cu/CF catalyst, and the bimetallic Co_xCu_y/CFs could produce CO and HCOOH. Metallic Cu owns relatively strong binding energies of *COOH and *CO intermediates compared to pure metallic Co, and these intermediates could be stabilized and further reduced to hydrocarbons or alcohols (Duan et al., 2018; Mun et al., 2019). In Co_xCu_y/CF samples, the catalytic behavior of metallic Cu was totally altered *via* fusing it with Co composition within the same nanoparticles. The binding energies of *COOH and *CO intermediates were weakened enough to be released from the catalyst surface, increasing the tendency toward HCOOH and CO production.

The electrochemical active surface area and the conductivity property of these five samples were also measured *via* double-layer capacitance (C_{dl}) and electrochemical impedance spectroscopy (EIS). Compared with Co/CFs (31.5 mF cm^{-2}), Cu/CFs (17.5 mF cm^{-2}), CoCu/CFs (30.0 mF cm^{-2}), and $CoCu_3$/CFs (21.5 mF cm^{-2}), Co_3Cu/CFs have a much higher C_{dl} value of 45.5 mF cm^{-2} (**Supplementary Figure S13**), manifesting the larger ECSA and more active sites for CO_2 reduction (Yang et al., 2020b; Hao et al., 2022). In addition, the EIS curves in **Figure 5B** prove that Co_3Cu/CFs show a relatively small impedance than those of the other samples, which is beneficial to faster electron transport as well as better conductivity (Wei et al., 2022; Liu et al., 2014). The larger ECSA and good conductivity of Co_3Cu/CFs is consistent with its higher current densities in LSV and electrolysis tests. As illustrated in **Figure 5C**, Co_3Cu/CFs possess highly graphitized and multi-level porous carbon nanofibers, which can accelerate the electron transmission and expose abundant bimetallic Co–Cu sites for CO_2 reduction, eventually leading to the remarkable partial current densities for C1 products.

CONCLUSION

In summary, an efficient Co_3Cu/CF catalyst was created with bimetallic Co–Cu nanoparticles evenly distributed within porous carbon nanofibers, which exhibited superior catalytic activities in CO_2 reduction. A total 97% total faradaic efficiency of CO and HCOOH could be achieved with the Co_3Cu/CFs catalyst at −0.8 V_{RHE} cathode potential in a 0.5 M $KHCO_3$ electrolyte. In addition, Co_3Cu/CFs could also bring forth a maximum 78.1 mA cm^{-2} partial current density for C1 production and maintain 60-h of stability in long-term electrolysis. In Co_3Cu/CFs catalysts, the doping of metallic Cu with Co can decrease the binding energies of key intermediates and increase the selectivity of CO and HCOOH. Moreover, the hierarchically porous carbon nanofibers are in favor of electron transmission and exposing active sites for CO_2 electroreduction. Consequently, this effective strategy of composition tuning along with a tailored structure might inspire the design and preparation of robust catalysts for CO_2 electroreduction.

DATA AVAILABILITY STATEMENT

The original contributions presented in the study are included in the article/**Supplementary Material**, further inquiries can be directed to the corresponding authors.

AUTHOR CONTRIBUTIONS

All authors listed have made a substantial, direct, and intellectual contribution to the work and approved it for publication.

FUNDING

This work was supported by the National Natural Science Foundation of China (22172099, 21975162, and 51902209), the Natural Science Foundation of Guangdong Province (2020A1515010840), and Shenzhen Science and Technology Program (Grant Nos. JCYJ20200109105803806, RCYX20200714114535052, RCBS20200714114819161, and JCYJ20190808111801674).

SUPPLEMENTARY MATERIAL

The Supplementary Material for this article can be found online at: https://www.frontiersin.org/articles/10.3389/fchem.2022.904241/full#supplementary-material

REFERENCES

Appel, A. M., Bercaw, J. E., Bocarsly, A. B., Dobbek, H., DuBois, D. L., Dupuis, M., et al. (2013). Frontiers, Opportunities, and Challenges in Biochemical and Chemical Catalysis of CO2 Fixation. *Chem. Rev.* 113 (8), 6621–6658. doi:10.1021/cr300463y

Appel, A. M., and Helm, M. L. (2014). Determining the Overpotential for a Molecular Electrocatalyst. *ACS Catal.* 4, 630–633. doi:10.1021/cs401013v

Benson, E. E., Kubiak, C. P., Sathrum, A. J., and Smieja, J. M. (2009). Electrocatalytic and Homogeneous Approaches to Conversion of CO2to Liquid Fuels. *Chem. Soc. Rev.* 38, 89–99. doi:10.1039/B804323J

Bonin, J., Maurin, A., and Robert, M. (2017). Molecular Catalysis of the Electrochemical and Photochemical Reduction of CO2 with Fe and Co

Metal Based Complexes. Recent Advances. *Coord. Chem. Rev.* 334, 184–198. doi:10.1016/j.ccr.2016.09.005

Chen Jia, C., Li, S., Zhao, Y., Hocking, R. K., Ren, W., Chen, X., et al. (2021). Nitrogen Vacancy Induced Coordinative Reconstruction of Single-Atom Ni Catalyst for Efficient Electrochemical CO 2 Reduction. *Adv. Funct. Mater.* 31, 2107072. doi:10.1002/adfm.202107072

Cheng, Z., Wang, X., Yang, H., Yu, X., Lin, Q., Hu, Q., et al. (2021). Construction of Cobalt-Copper Bimetallic Oxide Heterogeneous Nanotubes for High-Efficient and Low-Overpotential Electrochemical CO2 Reduction. *J. Energ. Chem.* 54, 1–6. doi:10.1016/j.jechem.2020.04.018

Duan, Y.-X., Meng, F.-L., Liu, K.-H., Yi, S.-S., Li, S.-J., Yan, J.-M., et al. (2018). Amorphizing of Cu Nanoparticles toward Highly Efficient and Robust Electrocatalyst for CO2 Reduction to Liquid Fuels with High Faradaic Efficiencies. *Adv. Mater.* 30, 1706194. doi:10.1002/adma.201706194

Duan, Y. X., Zhou, Y. T., Yu, Z., Liu, D. X., Wen, Z., Yan, J. M., et al. (2021). Boosting Production of HCOOH from CO 2 Electroreduction via Bi/CeO X. *Angew. Chem. Int. Ed.* 60, 8798–8802. doi:10.1002/anie.202015713

Fu, H.-C., You, F., Li, H.-R., and He, L.-N. (2019). CO2 Capture and *In Situ* Catalytic Transformation. *Front. Chem.* 7, 525. doi:10.3389/fchem.2019.00525

Hao, Q., Liu, D.-X., Deng, R., and Zhong, H.-X. (2022). Boosting Electrochemical Carbon Dioxide Reduction on Atomically Dispersed Nickel Catalyst. *Front. Chem.* 9, 837580. doi:10.3389/fchem.2021.837580

Hori, Y., Vayenas, C. G., White, R. E., and Gamboa-Aldeco, M. E. (2008). *Electrochemical CO_2 Reduction on Metal Electrodes*. New York: Springer, 89–189. doi:10.1007/978-0-387-49489-0_342

Jeoung, J.-H., and Dobbek, H. (2007). Carbon Dioxide Activation at the Ni,Fe-Cluster of Anaerobic Carbon Monoxide Dehydrogenase. *Science* 318, 1461–1464. doi:10.1126/science.1148481

Jia, Y., Li, F., Fan, K., and Sun, L. (2022). Cu-based Bimetallic Electrocatalysts for CO2 Reduction. *Adv. Powder Mater.* 1, 100012. doi:10.1016/j.apmate.2021.10.003

Kim, D., Xie, C., Becknell, N., Yu, Y., Karamad, M., Chan, K., et al. (2017). Electrochemical Activation of CO2 through Atomic Ordering Transformations of AuCu Nanoparticles. *J. Am. Chem. Soc.* 139, 8329–8336. doi:10.1021/jacs.7b03516

Kumar, B., Asadi, M., Pisasale, D., Sinha-Ray, S., Rosen, B. A., Haasch, R., et al. (2013). Renewable and Metal-free Carbon Nanofibre Catalysts for Carbon Dioxide Reduction. *Nat. Commun.* 4, 2819. doi:10.1038/ncomms3819

Lin Jia, L., Sun, M., Xu, J., Zhao, X., Zhou, R., Pan, B., et al. (2021). Phase-Dependent Electrocatalytic CO 2 Reduction on Pd 3 Bi Nanocrystals. *Angew. Chem. Int. Ed.* 60, 21741–21745. doi:10.1002/anie.202109288

Liu, D., Guo, Q., Hou, H., Niwa, O., and You, T. (2014). PdxCoy Nanoparticle/Carbon Nanofiber Composites with Enhanced Electrocatalytic Properties. *ACS Catal.* 4, 1825–1829. doi:10.1021/cs5000153

Mun, Y., Lee, S., Cho, A., Kim, S., Han, J. W., and Lee, J. (2019). Cu-Pd alloy Nanoparticles as Highly Selective Catalysts for Efficient Electrochemical Reduction of CO2 to CO. *Appl. Catal. B: Environ.* 246, 82–88. doi:10.1016/j.apcatb.2019.01.021

Nichols, A. W., and Machan, C. W. (2019). Secondary-Sphere Effects in Molecular Electrocatalytic CO2 Reduction. *Front. Chem.* 7, 397. doi:10.3389/fchem.2019.00397

Qiao, J., Liu, Y., Hong, F., and Zhang, J. (2014). A Review of Catalysts for the Electroreduction of Carbon Dioxide to Produce Low-Carbon Fuels. *Chem. Soc. Rev.* 43, 631–675. doi:10.1039/C3CS60323G

Sharifian, R., Wagterveld, R. M., Digdaya, I. A., Xiang, C., and Vermaas, D. A. (2021). Electrochemical Carbon Dioxide Capture to Close the Carbon Cycle. *Energy Environ. Sci.* 14, 781–814. doi:10.1039/D0EE03382K

Sun, X. (2021). Achieving Selective and Efficient Electrocatalytic Activity for CO2 Reduction on N-Doped Graphene. *Front. Chem.* 9, 734460. doi:10.3389/fchem.2021.734460

Vasileff, A., Xu, C., Jiao, Y., Zheng, Y., and Qiao, S.-Z. (2018). Surface and Interface Engineering in Copper-Based Bimetallic Materials for Selective CO2 Electroreduction. *Chem* 4, 1809–1831. doi:10.1016/j.chempr.2018.05.001

Wei, S., Jiang, X., He, C., Wang, S., Hu, Q., Chai, X., et al. (2022). Construction of Single-Atom Copper Sites with Low Coordination Number for Efficient CO2 Electroreduction to CH4. *J. Mater. Chem. A.* 10, 6187–6192. doi:10.1039/D1TA08494A

Xie, L., Yu, X., Wang, S., Wei, S., Hu, Q., Chai, X., et al. (2021). A Multiscale Strategy to Construct Cobalt Nanoparticles Confined within Hierarchical Carbon Nanofibers for Efficient CO 2 Electroreduction. *Small* 18, 2104958. doi:10.1002/smll.202104958

Yang, H., Wu, Y., Li, G., Lin, Q., Hu, Q., Zhang, Q., et al. (2019). Scalable Production of Efficient Single-Atom Copper Decorated Carbon Membranes for CO2 Electroreduction to Methanol. *J. Am. Chem. Soc.* 141, 12717–12723. doi:10.1021/jacs.9b04907

Yang, H., Lin, Q., Wu, Y., Li, G., Hu, Q., Chai, X., et al. (2020a). Highly Efficient Utilization of Single Atoms via Constructing 3D and Free-Standing Electrodes for CO2 Reduction with Ultrahigh Current Density. *Nano Energy* 70, 104454. doi:10.1016/j.nanoen.2020.104454

Yang, H., Yu, X., Shao, J., Liao, J., Li, G., Hu, Q., et al. (2020b). *In Situ* encapsulated and Well Dispersed Co3O4 Nanoparticles as Efficient and Stable Electrocatalysts for High-Performance CO2 Reduction. *J. Mater. Chem. A.* 8, 15675–15680. doi:10.1039/d0ta03770b

Yang, N., Chen, D., Cui, P., Lu, T., Liu, H., Hu, C., et al. (2021). Heterogeneous Nanocomposites Consisting of Pt 3 Co alloy Particles and CoP 2 Nanorods towards High-efficiency Methanol Electro-oxidation. *SmartMat* 2, 234–245. doi:10.1002/smm2.1032

Yu, D., Gao, L., Sun, T., Guo, J., Yuan, Y., Zhang, J., et al. (2021). Strain-Stabilized Metastable Face-Centered Tetragonal Gold Overlayer for Efficient CO2 Electroreduction. *Nano Lett.* 21, 1003–1010. doi:10.1021/acs.nanolett.0c04051

Zhang, S., Kang, P., and Meyer, T. J. (2014). Nanostructured Tin Catalysts for Selective Electrochemical Reduction of Carbon Dioxide to Formate. *J. Am. Chem. Soc.* 136 (5), 1734–1737. doi:10.1021/ja4113885

Zhang, J., Sewell, C. D., Huang, H., and Lin, Z. (2021). Closing the Anthropogenic Chemical Carbon Cycle toward a Sustainable Future via CO 2 Valorization. *Adv. Energ. Mater.* 11, 2102767. doi:10.1002/aenm.202102767

Zhang, J., Zeng, G., Chen, L., Lai, W., Yuan, Y., Lu, Y., et al. (2022). Tuning the Reaction Path of CO2 Electroreduction Reaction on Indium Single-Atom Catalyst: Insights into the Active Sites. *Nano Res.* doi:10.1007/s12274-022-4177-x

Conflict of Interest: The authors declare that the research was conducted in the absence of any commercial or financial relationships that could be construed as a potential conflict of interest.

Publisher's Note: All claims expressed in this article are solely those of the authors and do not necessarily represent those of their affiliated organizations, or those of the publisher, the editors, and the reviewers. Any product that may be evaluated in this article, or claim that may be made by its manufacturer, is not guaranteed or endorsed by the publisher.